Different Interactions between the Two Sides of Purple Membrane with Atomic Force Microscope Tip

Sheng Zhong,[†,§] Hui Li,[†,§] Xin-yong Chen,[‡] En-hua Cao,[†] Gang Jin,*[,†] and Kun-sheng Hu*[,†]

Institute of Biophysics, Chinese Academy of Sciences, 15 Datun Road, Chaoyang District, Beijing 100101, China, and Laboratory of Biophysics and Surface Analysis, School of Pharmacy, The University of Nottingham, University Park, Nottingham NG7 2RD, United Kingdom

Received October 23, 2006. In Final Form: January 16, 2007

Atomic force microscopy (AFM) is known to be capable of measuring local surface charge density based on the DLVO model. However, it has failed to distinguish charge density difference between the extracellular and cytoplasmic sides of purple membrane (PM) in previous studies. In this paper, tapping-mode AFM with thioglycolate-modified tips was used to image PM in buffers of different salt concentrations. When imaged in 25 mM KCl buffer, the topography of membranes appeared to be of two different types, one flat and the other domelike. Such a difference was not observed in buffers of high salt concentrations. This suggests that the topography variation results from differences in electrostatic interaction between the AFM tip and the different membrane surfaces. With images of papain-digested PM and high-resolution images of membrane surface structure, we proved that the membrane surfaces with flat topography were on the extracellular side while the surfaces with domelike topography were on the cytoplasmic side. Hence, this provides a straightforward method to distinguish the two sides of PM without the requirement of high-resolution imaging. Force−distance curves clearly demonstrated the different tip−sample interactions. The force curves recorded on the extracellular side of PM were consistent with the DLVO model, so its surface charge density can be estimated well. However, the curves recorded on the cytoplasmic side had a much longer decay length, which is supposed to be relevant to the flexibility of the C-terminus of bacteriorhodopsin (bR).

Introduction

Nowadays, atomic force microscopy (AFM) has been widely applied in biological study due to its powerful ability to work in a liquid environment with high resolution down to submolecular levels. AFM has revealed the surface structure of purple membrane (PM) with 0.5 nm resolution, consisting of the sole protein bacteriorhodopsin (bR) molecules packed in two-dimensional (2D) hexagonal lattice as trimers.[1−3] The photobleaching process of PM in the presence of hydroxylamine and its denaturation induced in high pH buffers have also been studied with AFM.[4,5]

AFM uses a very soft cantilever end-mounted with a sharp tip to sense the interactions between the tip and the sample surfaces. When imaging in buffer, if both the tip and the sample surfaces are similarly charged, there will be a repulsive electrostatic interaction existing between them. The strength depends on the surface charge density of the sample and tip, as well as the buffer conditions.[6] When imaged in low salt concentration buffers, a strong double layer force will affect the measured height of PM[7] and other surface-charged samples.[8] High-resolution imaging of PM can only be obtained in buffers of high salt concentration which screen off the electrostatic interaction between the AFM tip and the PM surface.[3]

The interactions between the AFM tip and the sample surface in solution can be described in a model developed by Derjaguin, Landau, Verway, and Overbeek (DLVO), which considers only electrostatic repulsive and Van der Waals attractive forces.[9,10] By fitting the force−distance curves obtained with AFM to the DLVO model, the surface charge density can be determined,[11−13] or a relative surface charge density of different surfaces can be measured.[14] A number of groups have measured the surface charge density and Debye length as a function of pH, electrolyte type, and concentration, and found good agreement with the standard DLVO model for measurement over hard surfaces.[15−18] A similar method has also been used to detect the surface charge density of PM[7,11,14] and surface potentials.[19,20] A surface charge density of about 0.05 C/cm^2 was obtained with no difference between the cytoplasmic (CP) and extracellular (EC) sides of PM.

However, the surface charge density of PM is still under debate. Since the structure of bR and lipids in PM has been well-

* To whom correspondence should be addressed. Tel: +86-10-6488-8428, E-mail: Gajin@imech.ac.cn (G. J.); or Tel: +86-10-64888580, Fax: +86-10-6487-1293, E-mail: huks@ibp.ac.cn (K.-s. H.).

† Chinese Academy of Sciences.

‡ The University of Nottingham.

§ The two authors contribute to the paper equally.

(1) Müller, D. J.; Schabert, F. A.; Büldt, G.; Engel, A. *Biophys. J.* **1995**, *68*, 1681−1686.

(2) Müller, D. J.; Fotiadis, D.; Scheuring, S.; Müller, S. A.; Engel, A. *Biophys. J.* **1999**, *76*, 1001−1111.

(3) Kienbergera, F.; Stroha, C.; Kada, G.; et al. *Ultramicroscopy* **2003**, *97*, 229−237.

(4) Möller, C.; Büdt, G.; Dencher, N. A.; Engel, A.; Müller, D. J. *J. Mol. Biol.* **2000**, *301*, 869−879.

(5) Li, H.; Chen, D. L.; Zhong, S.; Xu, B.; Han, B. S.; Hu, K. S. *J. Phys. Chem. B* **2005**, *109*, 11273−11278.

(6) Butt, H. J. *Biophys. J.* **1991**, *60*, 777−785.

(7) Müller, D. J.; Engel, A. *Biophys. J.* **1997**, *73*, 1633−1644.

(8) Rossell, J. P.; Allen, S.; Davies, M. C.; Roberts, C. J.; Tendler, S. J. B.; Williams, P. M. *Ultramicroscopy* **2003**, *96*, 37−46.

(9) Israelachvili, J. L. *Intermolecular and surface forces*; Academic Press: London, 1992.

(10) Cappella, B.; Dietler, G. *Surf. Sci. Rep.* **1999**, *34*, 1−104.

(11) Butt, H. J. *Biophys. J.* **1992**, *63*, 578−582.

(12) Rotsch, C.; Radmacher, M. *Langmuir* **1997**, *13*, 2825−2832.

(13) Johnson, A. S.; Nehl, C. L.; Mason, M. G.; Hafner, J. H. *Langmuir* **2003**, *19*, 10007−10010.

(14) Heinz, W. F.; Hoh, J. H. *Biophys. J.* **1999**, *76*, 528−538.

(15) Ducker, W. A.; Senden, T. J.; Pashley, R. M. *Nature (London)* **1991**, *353*, 239−241.

(16) Butt, H. J. *Biophys. J.* **1991**, *60*, 1438−1444.

(17) Hillier, A. C.; Kim, S.; Bard, A. J. *J. Phys. Chem.* **1996**, *100*, 18808−18817.

(18) Raiteri, R.; Gratarola, M.; Butt, H. J. *J. Phys. Chem.* **1996**, *100*, 16700−16705.

(19) Hartley, P.; Matsumoto, M.; Mulvaney, P. *Langmuir* **1998**, *14*, 5203−5209.

(20) Knapp, H. F.; Mesquida, P.; Stemmer, A. *Surf. Interface Anal.* **2002**, *33*, 108−112.

10.1021/la0631062 CCC: $37.00
Published on Web 03/15/2007

determined, it is possible to estimate the net charge per bR on each side of PM according to the apparent pK_a values of amino acid residues and lipids.[21] Calculation shows that the CP side is more negative than the EC side in buffers with pH ranging from 4 to 9. The bR molecule functions as a light-driven proton pump. Upon light excitation, bR undergoes a photocycle accompanied by a net transport of one proton from the CP side to the EC side.[22] The higher surface charge density on the CP side of PM should be relevant to the proton pump function of bR through attracting protons to enrich to a high local proton concentration near the CP surface, by which the proton uptake may be affected.[23] Many efforts have been made to measure the surface charge density of PM, but the results are inconsistent, as reviewed by Jonas.[21] Alexiev et al. measured a negative charge density of about 2.5 elementary charges per bR on the CP side and about 1.8 elementary charges per bR on the EC side by the use of covalently bound pH indicators.[23] However, there has been no report of the different surface charges between the two sides of PM detected by AFM.

In addition, for the experiments of bR unfolding by single molecular force spectrum[24,25] and in situ observation of the surface structure changes of PM treated by detergent, an easy method is needed to distinguish the orientations of PM in situ. Normally, it is done according to high-resolution imaging of the PM surface. However, high-resolution imaging is not always accessible. Recently, Voïtchovsky et al. proposed a method to solve the problem by phase imaging in low-concentration buffer, by which they measured different stiffness and lipid mobility of PM.[26] However, the formation of phase contrast was not explained.

Moreover, bR has a relatively long tail at its C-terminus (from Glu232 to Ser248), which is not accessible to X-ray diffraction (XRD) or electron microscopy (EM) structure. NMR experiments[27] and molecular dynamics simulations[28] have evidenced that the first part of the tail is constrained to the membrane via a salt bridge while the rest of the tail is freely movable from Pro236 to the end. Since the freely movable tail contains three negative charges (Glu237, Asp242, and Ser248) at neutral pH, it has electrostatic interaction with AFM tip. However, the tail detail has not been reported either in high-resolution AFM images or surface-charge measurement by AFM.

In the present study, we modified AFM tips with thioglycolate to enlarge the electrostatic interaction by achieving a more negatively charged tip surface and imaged PM in neutral buffers of low KCl concentration. Two types of membrane sheets with different surface topography, flat and domelike, were observed. After the C-terminus of bR was cut off by papain digestion, all membranes showed a flat surface, suggesting that the domelike surface was the CP side of PM. This conclusion was further proven by high-resolution AFM images. The force−distance ($f-d$) curves recorded on the EC side were consistent with the prediction by the DLVO model, while the $f-d$ curves recorded on the CP side were not. It is supposed that the extraordinary interactions between the CP side and the AFM tip are related to the freely movable tails of bR molecules.

Materials and Methods

Materials. Culture of *Halobacterium halobium* and isolation of PM were carried out as described previously.[29,30] Purified PM was suspended in double-distilled water and stored at 4 °C. The main buffers used in the experiments consisted of 10 mM Tris and KCl of different concentrations. The pH value was adjusted to 7.6 with HCl. Mercaptoacetic acid calcium salt (S534889) was purchased from Sigma-Aldrich and distilled to 10 μM with ultrapure water.

Papain Proteolysis of bR. The bR was digested with papain type IV (Baker) following the protocol of Müller et al.[31] Briefly, papain was incubated in pH 7.0 activation buffer consisting of 1 mM EDTA, 0.6 mM 2-β mercaptoethanol, and 5 mM cysteine−HCl at 0.1 mg/mL concentration for 30 min at room temperature. bR (300 μg in 300 μL activation buffer) was digested by shaking at 37 °C with 15 μL activated papain for 3 h. Control samples were treated in the same way except in the absence of papain. Digested samples were diluted in a pH 6.8 buffer consisting of 1 M NaCl and 10 mM Tris-HCl, and collected by centrifugation at 30 000 *g* for 15 min at 4 °C. The procedure of centrifugation was repeated three times to remove the papain completely. Finally, the pellet was resuspended in ultrapure water to a final concentration of about 1 mg/mL.

AFM Sample Preparation. For AFM experiments, PM samples were diluted to 1 μg/μL in buffers of different KCl concentrations. A 10 μL aliquot of PM suspension was pipetted onto a freshly cleaved mica surface and left in air for 3−5 min to allow absorption. The sample was then mounted under the microscope without rinsing unless particularly indicated. 30 μL of the same buffer was injected, and the equipment was allowed to stand for 30 min to reach thermal equilibrium.

AFM Tip Modification. In AFM experiments, the oxidation-sharpened silicon−nitrogen tips were used for high-resolution scanning (the NP−S model, Veeco Instruments, U.S.A.). For modification of calcium mercaptoacetate ($(HSCH_2\ COO)_2Ca$) to increase the negative charge, the tips were first coated with 20 nm gold. The gold-coated tip was then cleaned by immersion in 0.1 N HCl for a few seconds and then rinsed with 10 mM sodium phosphate buffer (pH 7.2). After that, the cleaned tip was dipped into 3.2 mM calcium mercaptoacetate solution for 1 h at room temperature. Finally, the tip was rinsed with 10 mM sodium phosphate buffer (pH 7.2) and then ultrapure water to remove unbound mercaptoacetic acid. The cantilever deflection sensitivity was calibrated by force curves obtained on a mica surface (values were found around 50 nm/V), and the spring constant was determined with the thermal-tune method[32] after completion of all force measurements (values were found around 0.06 N/m).

Tapping-Mode AFM. AFM experiments were performed with a commercial microscope (NanoScope IIIa Multi-Mode AFM, Veeco Instruments) with a 13 μm scanner and a liquid cell. Most PM topography images were obtained with tapping mode. Due to the nature of acoustic tapping mode in liquid, multiple resonant peaks were observed during "cantilever tune". A drive frequency at a peak around 8.5 kHz, which is the closest to the cantilever resonance, was selected. Drive amplitude was adjusted so that the tip oscillation amplitude was 1−2 V (rms value and corresponding to about 40 nm for 1 V). Gains were set to the highest value but do not cause oscillation of tip (usually 1.5 to 2).

Force−Distance Measurement. After tapping-mode AFM imaging, the tip was disengaged and raised to about 5 μm above the sample surface, and the microscope was switched to contact mode before being engaged again. The setpoint value was carefully minimized for a low-force contact-mode imaging. The lateral shift

(21) Jonas, R.; Kautalos, Y.; Ebrey, T. G. *Photochem. Photbiol.* **1990**, *52*, 1162−1177.
(22) Haupts, U.; Tittor, J.; Oesterhel, D. *Annu. Rev. Biophys. Biomol. Struct.* **1999**, *28*, 367−99.
(23) Alexiev, T.; Marti, T.; Heyn, M. P.; Khorana, H. G.; Scherrert, P. *Biochemistry* **1994**, *33*, 298−306.
(24) Oesterhelt, F.; Oesterhelt, D.; Pfeiffer, M.; Engel, A.; Gaub, H. E.; Müller, D. J. *Science* **2000**, *288*, 143−146.
(25) Kessler, M.; Gottschalk, K. E.; Janovjak, H.; Müller, D. J.; Gaub, H. E. *J. Mol. Biol.* **2006**, *357*, 644−654.
(26) Voïtchovsky, K.; Contera, S. A.; Kamihira, M.; Watts, A.; Ryan, J. F. *Biophys. J.* **2006**, *90*, 2075−2085.
(27) Engelhard, M.; Finkler, S.; Metz, G.; Siebert, F. *Eur. J. Biochem.* **1996**, *235*, 526−533.
(28) Edholm, O.; Berger, O.; Jähnig, F. *J. Mol. Biol.* **1995**, *250*, 94−111.
(29) Oesterhelt, D.; Stoeckenius, W. *Methods Enzymol.* **1974**, *31*, 667−678.
(30) Xu, B.; Chen, D. L.; Hu, K. S. *Prog. Biochem. Biophys.* **2002**, *29*, 827−831.
(31) Müller, D. J.; Schoenenberger, C. A.; Büldt, G.; Engel, A. *Biophys. J.* **1996**, *70*, 1796−1802.
(32) Hutter, J. L.; Bechhoefer, J. *Rev. Sci. Instrum.* **1993**, *64*, 1868−1873.

caused by the disengage/engage procedure was found to be less than 1 μm, and hence, it was not difficult to relocate the membranes previously observed in tapping mode. Force−distance curve measurements were then performed on the selected membranes by ramping the tip in the vertical direction with a size of 100 nm at 4 Hz. At least 20 curves were collected on each surface position.

Results

Two Types of PM Surface Topography Observed in Tapping-Mode AFM. Figure 1 shows PM topographies imaged in different buffers and different tapping-mode amplitude setpoints. First, images were recorded in 25 mM KCl buffer with the highest amplitude setpoint (typically 1.8 V for free amplitude of 2 V). A typical image is shown in Figure 1a, where about 16 membrane sheets are seen. Among these sheets, 5 of them have flat surfaces, while the others have domelike surfaces. In the right panel, the profiles of 2 representative membranes are displayed to show the differences more clearly. The green line shows the flat surface with an average thickness measured about 7.1 nm, with a variation at different positions along the line of less than 0.3 nm. The red line shows the profile of a domelike surface with height measured 19.7 nm at the center while about 6 nm at the edge.

The PM sheets shown in Figure 1a could be repeatedly imaged without significant change to their lateral shapes. However, the height features were sensitive to the imaging parameters, especially the setpoint value. Following a decrease of amplitude setpoint (increase of tapping strength), the domelike surfaces gradually became flat, while the originally flat surfaces did not show significant change except a slight decrease in height. In Figure 1b, which was recorded at a setpoint of 1.7 V, the measured thickness of the flat membrane slightly decreased to 5.8 nm, and the measured height of the domelike membrane decreased to 11.6 nm at the center. When the setpoint value was further decreased to 1.6 V, all membranes showed a thickness about 6 nm, and the original difference between the two types of membranes totally disappeared because the originally domelike surfaces became completely flat (Figure 1c). The difference was restored when the setpoint value was increased back, as shown in Figure 1d, which was recorded at a setpoint of 1.8 V.

The dependence of topography on the imaging setpoint value indicates that the domelike feature is due to variation of tip−sample interactions instead of real surface morphology. This was further proven by imaging in buffers with different KCl concentrations. After recording the image shown in Figure 1d, a drop of 20 μL of 250 mM KCl buffer was injected, resulting in a final KCl concentration of about 80 mM. As shown in Figure 1e, even with the lightest tapping, no domelike membrane surface was observed. All membrane sheets showed a flat surface with height measured about 5.4 nm, close to the actual thickness of PM determined in other studies.[2] The membrane topography had little change when the setpoint value was varied. Furthermore, the procedure was reversible, as observed in another experiment (images not shown), where we first imaged PM in 25 μL 50 mM KCl buffer, and the results were quite similar to those shown in Figure 1e. We then injected 25 μL double-distilled water into the liquid cell, which resulted in a final KCl concentration of about 25 mM, and the obtained images showed similar features to those shown in Figure 1a,d. This also excluded the suspicion that the domelike topography of PM might come from pollutants on the sample surface.

Different Tip−Sample Interactions Shown in Force−Distance Curves. Our hypothesis that the different topographies shown in Figure 1a were induced by different tip−sample interactions rather than real surface morphology was supported by the force−distance measurement. After tapping-mode imaging in 25 mM KCl buffer, we raised the tip, changed the microscope to contact mode, and engaged again. We found that the images collected with contact mode also displayed the same two types of topographic features like those shown in tapping mode, but the membranes were easier to destroy under relatively high imaging force. After locating the membrane patches that we interested in, the $f-d$ curves were recorded.

Figure 2a shows the extending part of the $f-d$ curves taken on mica and membrane with flat and domelike surfaces, which were in 25 mM KCl buffer. Each curve represents an average of 10 $f-d$ curves, with proper offsets added for a clearer display. The force curve recorded on the domelike membrane (top of Figure 2a) shows the effect of long-range repulsive forces, which deflects the cantilever smoothly as the distance between the tip and the membrane decreases. However, the force curve recorded on the flat membrane (middle of Figure 2a) indicates a short-range repulsive force, which increases sharply following a decrease of the tip−sample distance. The force curve recorded on the mica surface (bottom of Figure 2a) demonstrates an even shorter range in the repulsive fore. The red line in each curve shows fitting to an exponential decay function. The fitting starts from a distance of about 2 nm away from the sample surface and results in decay lengths of 20 nm on the domelike membrane, 2.1 nm on the flat membrane, and 2.8 nm on mica.

Figure 2b shows $f-d$ curves measured on the same surfaces after adding 20 μL of 250 mM KCl buffer. Exponential decay fitting (red lines) gives a much shorter decay length on the domelike membrane (2.3 nm) in comparison with that measured in low KCl concentration buffer but close to that measured on the flat membrane (2.5 nm) and on mica (1.8 nm). The decay length's strong dependence on the buffer's ion concentration suggests that the repulsive force originates from electrostatic interaction between the AFM tip and the PM surface.

Imaging Papain-Digested PM. As shown above, the native PM appear in two types of surface topographic features in buffers of low KCl concentrations, which are not "true" different topographies but imaging artifacts induced by different tip−sample interactions. The dependence on salt concentration indicates the electrostatic nature of the interaction. Because the two sides of PM have different surface charge densities[21] and the adsorption of PM onto mica surface is randomly oriented, it is reasonable to relate the two types of topography to the two sides of PM. In order to test the hypothesis, we used papain to cut off the C-terminus of bR and then imaged the digested PM under the same conditions.

The limited proteolysis of bR by papain is shown in Figure 3a. The intact bR migrates on the SDS-PAGE gel with an apparent molecular mass of approximately 26 kDa (Figure 3a, lane 1). After digestion by papain, the prominent protein species migrated with a slightly decreased electrophoretic mobility (Figure 3a, lane 2). Previous studies have determined that the cleavage occurs primarily between Gly-231 and Glu-232 by papain digestion,[33,34] shortening bR by 17 amino acids at the C-terminus. Five negative surface charges per bR (including Ser248) are removed with the loss of the 17 amino acids according to the folding model of bR.[21]

The digested PM was then imaged with the same method mentioned above in 25 mM KCl buffer. Typical topography was shown in Figure 3b, in which 15 membrane sheets can be seen. In spite of some debris on the surface, which may result from

(33) Liao, M. J.; Khorana, H. G. *J. Biol. Chem.* **1984**, *259*, 4194−4199.
(34) Fimmel, S.; Choli, T.; Dencher, N. A.; Buldt, G.; Wittmann-Liebold, B. *Biochim. Biophys. Acta* **1989**, *978*, 231−40.

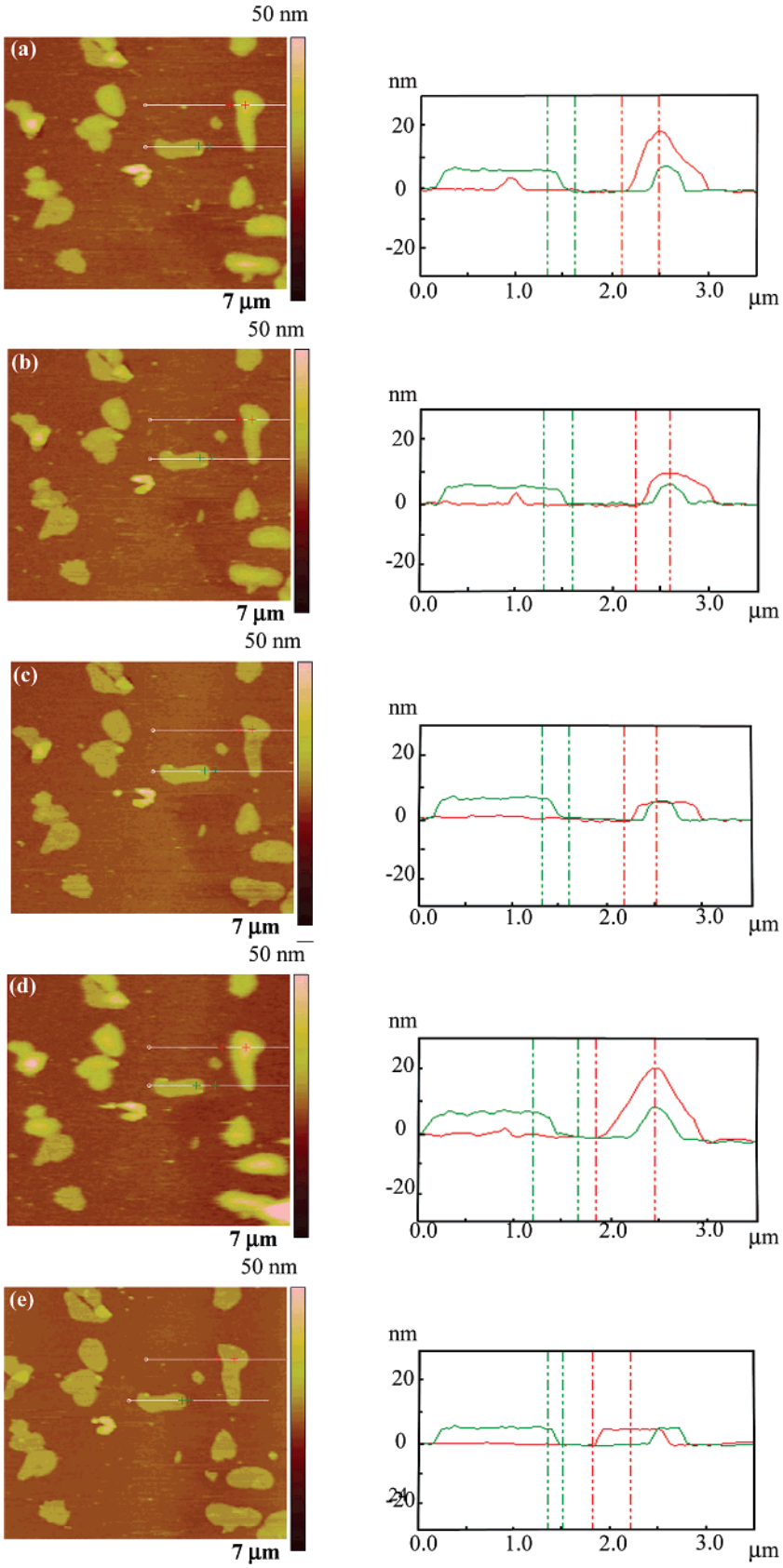

Figure 1. Tapping-mode AFM topography of PM sheets recorded in 25 mM KCl buffer setpoint values of 1.8 V (a), 1.7 V (b), 1.6 V (c), and 1.8 V (d), respectively, and recorded after adding 250 mM KCl buffer (e). The profiles at two selected lines as indicated in the images are shown (in red and green) in the corresponding line plots.

PM aggregation during digestion and repeated centrifugation, all of the membrane sheets show a flat surface with thickness of about 5.3 nm, and the topography changed very little following the change of imaging setpoint. No domelike membrane like those shown in Figure 1a was ever observed. Therefore, we conclude that the membranes with domelike topography observed in 25 mM KCl buffer are PM with its CP side facing upward, while the other membranes with flat surface should be PM with

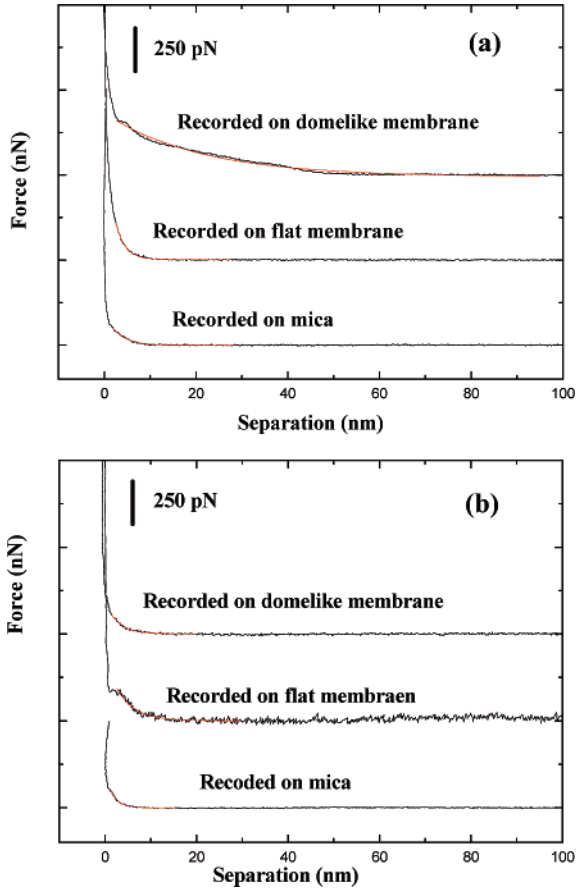

Figure 2. Force curves obtained on two types of membrane surfaces and a mica surface in 25 mM KCl buffer (a) and after adding 20 μL 250 mM KCl solution into the buffer (b). Only the extending part of the force curves are shown. Each curve represents an average of ten measurements. The red lines indicate the fitting to an exponential decay function.

EC side facing upward. Thus, AFM imaging of PM in low KCl concentration buffers with negatively charged tips provides a simple method to distinguish the CP and EC sides of PM.

Different Surface Structures of PM Revealed by AFM Imaging with Untreated Tips. Under proper control of experimental conditions, AFM can obtain high-resolution images of PM.[2,3,5] In the experiments mentioned above, the AFM tip was modified with thioglycolate in order to enhance the tip surface's negative charge. However, this modification significantly declined the tip's sharpness and hence prevented us from obtaining high-resolution images.

By using unmodified tips, we did obtain high-resolution images of PM. Figure 4a shows the topography of PM imaged with an untreated NP−S tip (without gold coating) in 25 mM KCl buffer. In the image, two types of membrane surfaces can be recognized, although the contrast is much lower in comparison with that in Figure 1a. The two membrane patches on the right side with domelike surfaces should be with the CP side facing up, and the others with flat surfaces should be with the EC side facing up.

Since high-resolution imaging of PM requires high salt concentration to mask surface charges so that the tip−sample distance can be minimized,[2] after recording the image shown in Figure 4a, we injected another 20 μL of 600 mM KCl buffer, which resulted in a final KCl concentration of 300 mM, and changed the microscope to contact mode to image the same area. Figure 4b shows the deflection image of the area indicated by the square in Figure 4a, which covers both the flat (the left side in Figure 4b) and domelike (the right side in Figure 4b) surfaces.

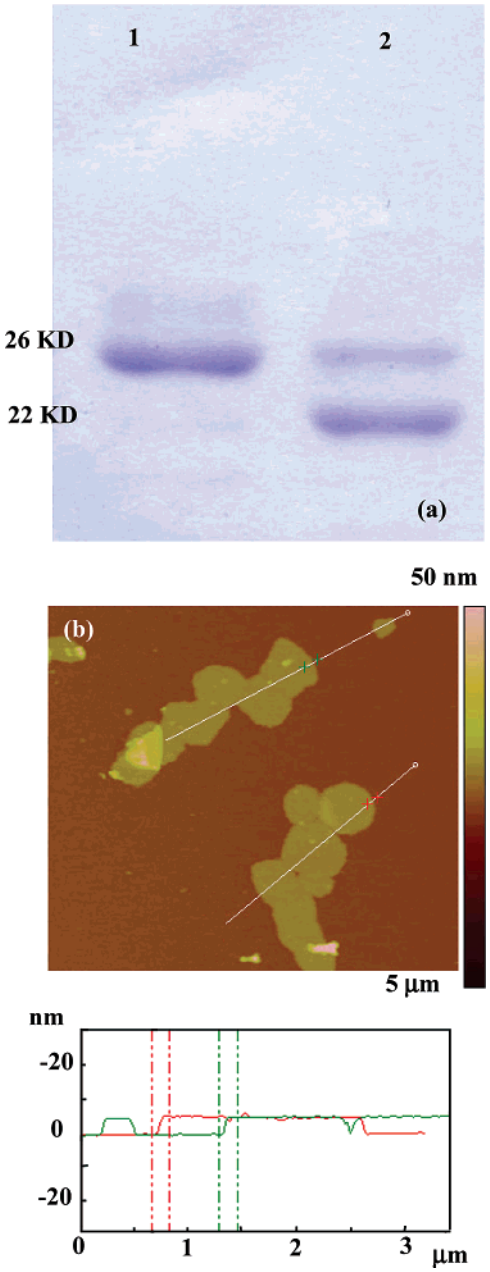

Figure 3. (a) Analysis of native (lane 1) and papain-digested (lane 2) PM on SDS-PAGE gel, and the digestion was actually not completed for a part of BR intact as a 26 kD band in lane 2. (b) Tapping-mode AFM topography image and line profiles of papain-digested PM in 25 mM buffer. All membranes have a flat surface.

The deflection image was adopted because it is the "error" image in the constant-force mode, more sensitive to the high-frequency components than the low-frequency ones, and works like a low-pass filter with the topographic details significantly enhanced. The lattice structure is clearly seen in Figure 4b, particularly in the right-side area where the surface is smoother. In previous studies, Müller et al. assigned the rougher doughnut unit side and the smoother three-dot unit side to the CP and EC sides, respectively, according to their excellent high-resolution images and antibody verification of the orientations.[26] Following their results, the right-side part in Figure 4b should be the CP side of PM, while the left-side part should be the EC side. This agrees with our hypothesis that the domelike surface in low KCL concentration buffer is the CP side while the flat surface is the EC side. A "zoom-in" image with much higher resolution of the right-side part is shown in Figure 4c. Three circles indicate the

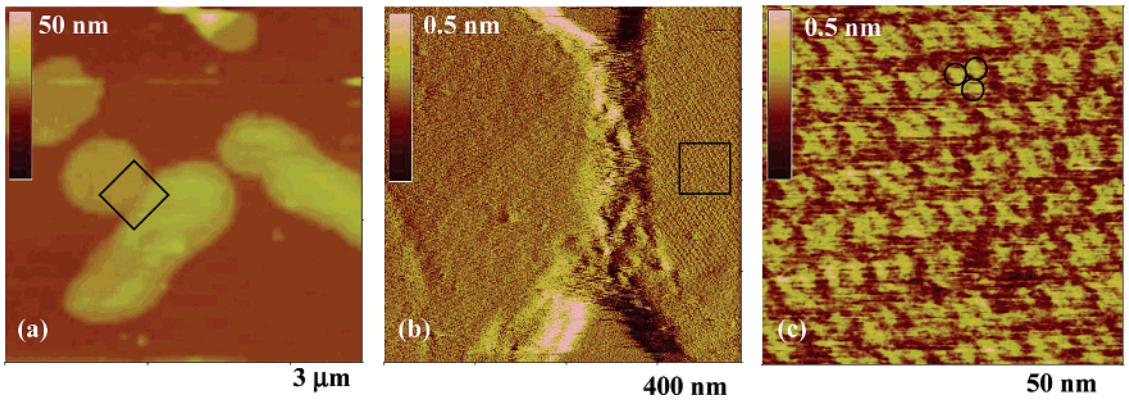

Figure 4. Topography of PM imaged in 25 mM buffer with an "untreated" AFM tip and tapping mode (a), together with a contact mode "deflection" image (b) showing the square area in (a) after another 20 μL 600 mM KCl buffer was injected, and another "deflection" image (c) showing the square area in (b).

Table 1. Thickness of Purple Membranes with Their EC Sides Facing toward the Aqueous Solution Measured under Different KCl Buffer Concentrations and Different Setpoint Amplitudes[a]

concentration of KCl in buffer	thickness recorded with setpoint of 1 V (nm)	thickness recorded with setpont of 0.95 V (nm)	Debye length predicted by DLVO model (nm)	decay length by fitting $f-d$ curves to exponential decay function (nm)
25 mM	10.1 ± 1.1	7.6 ± 0.8	1.90	2.1
50 mM	7.5 ± 0.8	6.4 ± 0.5	1.35	1.5

[a] Each result represents average of at least ten membranes.

bR trimer. There is a slight distortion, which may be caused by repeat scanning.

Discussion

Distinguishing the Two Sides of PM. bR is asymmetrically oriented in PM for its proton pump function, and the kind of asymmetry is common for almost all of the membrane protein. However, despite its ubiquity, it is experimentally difficult to observe membrane asymmetry, and labeling techniques are generally required. In former studies of PM by AFM, there are two ways to identify the orientation of PM, by labeling with antibody[31] and by high-resolution imaging.[2,4] However, labeled PM will not be used to observe the in situ structural change of native PM, and the high-resolution imaging is not always accessible and sometimes can be misleading because it requires a very sharp tip stylus. So, a simple method is needed to identify the orientation of PM without labeling and without requiring high-resolution imaging.

Here, we present an easy method to identify the orientation of PM in low-salt buffer by the different electrical interaction of AFM tips with the EC and CP sides of PM. The difference can be clearly seen in topography, either flat or domelike. The AFM tip can be modified to be more negative charged in order to enhance the contrast; however, the modification is not always needed. It is hard to get the distinguishable contrast with a tip that is too sharp, but with a normal commercial tip, the difference is always observed. The method can be used to observe structural changes of PM treated by detergent and to unfold bR by force spectrum.

Just before our work, Voïtchovsky et al. presented a method to identify the orientation of PM by phase contrast in low salt buffer.[26] In our work, we also observed phase contrast in addition to the difference of observed topography (Supporting Information), with the domelike membrane to be darker in phase image than those of flat ones, which contrasted with the suggestion of Voïtchovsky et al. Moreover, it was claimed by Voïtchovsky et al. that the tip penetrated very easily through the whole membrane to reach the mica underneath, and they also obtained side-specific force spectroscopy, in which the force curve on the "EC" side decayed more slowly than that on the "CP" side, just contrary to our results (i.e., "EC" equal to CP and "CP" equal to EC in our outcomes). It was explained that the "EC" side is more resistant to the tip pressure. However, it is unlikely that the AFM tip had penetrated through the membrane with a force of about 2 nN.[24] Actually, the force curves on the EC surface of PM are rather similar to those on mica, and maybe it was misunderstood as penetration. Furthermore, a hole can be observed if the tip does penetrate through the membrane in an AFM experiment. If a tip with diameter of about 10 nm was used to penetrate through the membrane 5 nm to reach the mica surface, a hole of about 10 nm is supposed to be induced and the hole is unlikely to be healed in a short time. In the work of Oesterhelt et al.,[24] a hole can be observed even if only one bR protein was taken out of the membrane, which is less than 7 nm in diameter.

Force Curves on the EC Side of PM Fitting to DLVO Model. The force between two charged surfaces in electrolyte solution can be described by the DLVO model, which only concerned the electrostatic force and Van der Waals force. According to the DLVO model, the repulsive electrostatic force between the AFM tip and the sample surface can be described as

$$F(z) = \frac{2\pi\sigma_t\sigma_s R\lambda_D}{\epsilon_e\epsilon_0} e^{-z/\lambda_D} \quad (1)$$

where σ_t and σ_s are the surface charge densities of the tip and sample surfaces, respectively, and ϵ_e and ϵ_0 are the dielectric constant of solution and the vacuum permittivity, respectively. R is the effective radius of the tip, and Z is the distance between the tip and the sample. λ_D is the Debye length, given by

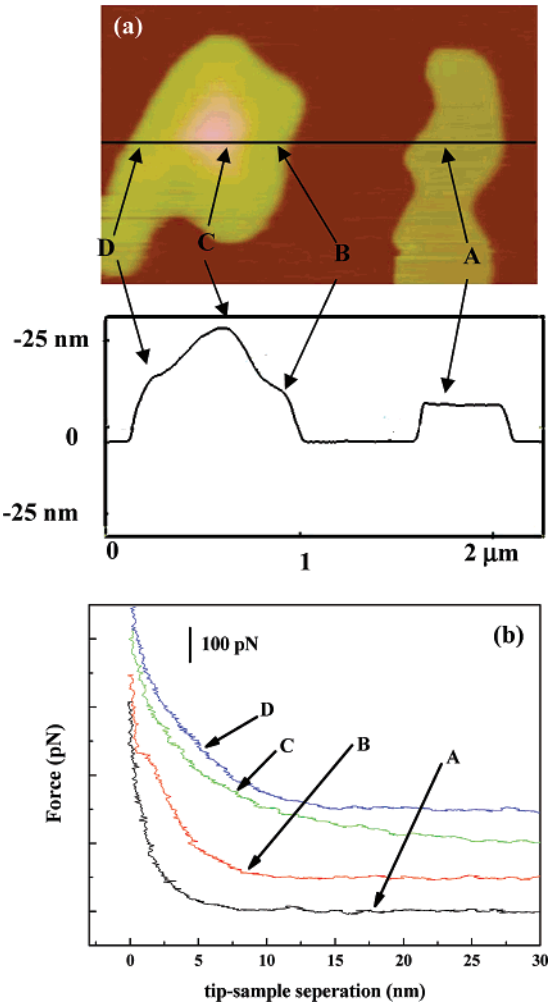

Figure 5. Topography (upper panel) and line profile (lower panel) of two PM sheets with different sides facing upward (a), imaged in 25 mM KCl buffer, with force curves (b) recorded at the four positions (A, B, C, and D) indicated in (a).

$$\lambda_D = \frac{0.304}{\sqrt{C}}\ \text{nm} \tag{2}$$

for a monovalent salt at 22 °C, where C is the concentration of the salt in mol/L.

From eqs 1 and 2, we can see that there would be a significant double-layer force between tip and sample when imaging in buffer of low salt concentrations due to a relatively large Debye length. Müller et al. have shown that, in AFM, this repulsion can make a contribution to the height measurement of the PM surface.[7] High-resolution images can only be obtained in buffer of high salt concentration of about 300 mM KCl.[2]

In our studies, the force curves recorded on the EC side show a very sharp decrease with the increase of tip−sample distance (Figure 2a, middle). Fitting the force curves with an exponential decay function results in a decay constant of about 2.1 nm, similar to the prediction by the DLVO model that gives a Debye length of about 1.9 nm.

The measured thickness also depends on the salt concentration and the amplitude setpoint. We imaged PM in KCl buffers of different concentrations (25 mM, 50 mM, and 250 mM, with Tris−HCl, pH 7.60) with setpoint amplitudes of 1 V and 0.9 V (free amplitude about 1.05 V). The measured values of membrane thickness (with the EC side toward the buffer) are given in Table 1. We can clearly see that the thickness of membranes decreases with the increase of KCl concentration, as well as the decrease of imaging amplitude. The results are consistent with previous studies.[7]

Theoretically, it is possible to calculate surface charge density by fitting $f-d$ curves to eq 1 if the tip radius and tip surface charge density are known.[7] Heizn et al. have also developed a method to measure the relative surface charge density by "force volume" measurement at different salt concentrations, which does not require prior knowledge of tip radius and tip charge.[14] They deduced the expression

$$\ln\left(\frac{\sigma_1}{\sigma_2}\right) = \frac{[(Z_1^{low} - Z_2^{low}) - (Z_1^{hi} - Z_2^{hi})]}{\lambda_{low} - \lambda_{hi}} \tag{3}$$

in which σ_1 and σ_2 represent the surface charge density of two materials (in the present cases, PM and mica, respectively). λ_{low} and λ_{hi} are the Debye lengths of two buffers. Z_i represents the Z position of the tip over an isoforce surface. We can replace Z_i by the membrane thickness $T_{membrane}$ as

$$T_{membrane} = Z_{membrane} - Z_{mica} \tag{4}$$

This yields

$$\ln\left(\frac{\sigma_{PM}}{\sigma_{mica}}\right) = \frac{T_{membrane}^{low} - T_{membrane}^{high}}{\lambda_{low} - \lambda_{high}} \tag{5}$$

It should be pointed out that the thickness of membrane in low- and high-concentration buffers must be measured with the same tip and the same tip−sample repulsive force. Heizn et al. used contact mode with contact-force scan, and hence, the same force is insured. Though in tapping mode the tip−sample interactive forces are more complex, we can still reasonably assume that eq 5 is valid to the first approximation, considering that the tip−sample interactions are dominated by the long-range repulsive force in very light tapping and that the equality of tip−sample interactive strength is insured by the same relative setpoint and free amplitude. On the basis of the results shown in Table 1, a relative surface charge density ($\sigma_{PM}/\sigma_{mica}$) of about 7 can be obtained. Previous studies have reported a negative charge density of about 0.02 e^-/nm^2 for the mica surface.[30] This leads to a charge density of ~0.14 e^-/nm^2 on the EC surface of PM, equal to about 1.6 charges per bR. Müller et al.[2] had obtained a surface charge density of PM of ~0.31 e^-/nm^2, about two times higher than ours. However, Müller's result might be an average of both the EC and CP sides of PM since he did not distinguish them in electrostatic force measurement, and actually, the decay of the force curve on the CP surface is not consistent with the DLVO model. Moreover, the accuracy of our result is also limited by the discrepancy between the measured decay length and the theoretical prediction (the Debye length) and the uncertainty of surface charge density of mica.

Domelike Topography of the CP Side of PM. Contrary to the flat surface of the EC side of PM, the CP side shows a domelike surface topography when imaged in buffer of low salt concentrations (Figure 1). The domelike topography is not a real surface structure but is induced by a strong electrostatic interaction. The interaction with longer decay length (Figure 2a, top), as a result of higher surface charge density on the CP side, introduces another factor to contribute to the domelike structure of the CP side, i.e., the so-called "size effect", which means the tip felt a stronger force at the center than at the edge when the tip was at the same high level above the CP side

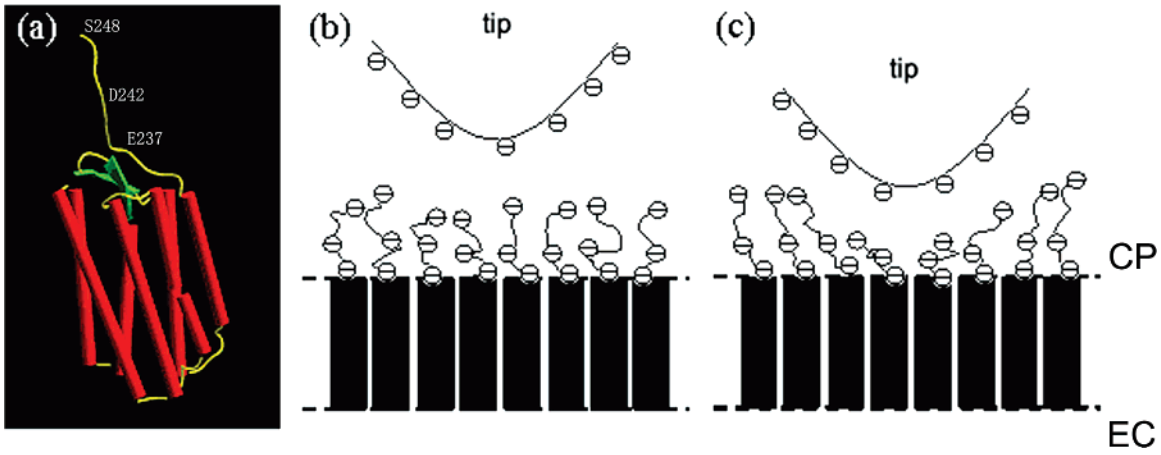

Figure 6. (a) A representative structure of seven α-helixes and C-terminus of bR. (b,c) Schematic shows conformation of the tails when the AFM tip is far from the PM surface (b) and near the surface (c).

membrane. Therefore, the observed thickness of membranes (measured from the highest position of the membrane to the mica surface) seems to be dependent on the size of the membrane. The longer decay the length is, the larger the effective tip−sample interaction area will be. The tip−sample interaction cannot be treated as a local interaction anymore when the decay length is longer than a certain value. The larger interaction area as the tip is on the center of the membrane will result in a stronger total interaction with a longer decay length in comparison with the case where the tip is on the edge of the membrane. This in turn forms the domelike topography artifact.

We observed that the *f*−*d* curves varied at different positions of the membrane. Figure 5a shows the topography of two membranes with different sides facing toward the solution and a line profile crossing the central part of the two membranes. After the image was obtained with tapping mode in 25 mM KCl buffer, we immediately changed the mode to contact, located the membranes, and then took force curves along the line by the "auto ramp" function provided by the instrument. Force curves at 40 surface points separated by 50 nm along the line were collected. For clarity, only 4 force curves on typical positions indicated in Figure 5a are selected to show in Figure 5b. The *f*−*d* curves recorded on the membrane at the right side of the image (the EC side of PM) were all similar to each other, as shown by curve A. However, the curves recorded at different positions on the CP side of PM (the membrane on the left-side of the image) varied very much. The curve recorded on the center of the membrane (C) has a stronger interaction and longer decay length than those recorded on the edge of the membrane (B and D). This indicates the size effect contributing to both the membrane topography and force curves.

The long decay length recorded on the CP side of PM does not fit the DLVO model. In the DLVO model, the decay length (the Debye length) only relates to the concentration of counterions in the buffer (eq 2). Because the domelike topography feature disappeared when imaging papain-digested PM, it is reasonable to assume a relationship between the deviant interaction and the C-terminus of bR.

The C-terminus has more than 10 amino acid residues from Pro236 to Ser248 and is flexible in liquid as shown in Figure 6a, which is the reason the structure of C-terminus cannot be obtained by XRD or TEM. The high mobility of the C-terminus has been verified by molecular dynamics simulation and ^{13}C NMR experiments.[27,28] Meanwhile, the flexible tail has three negatively charged residues (Glu237, Asp242, and Ser248) in neutral buffer. The flexibility of the negatively charged C-terminus tail would enhance the long-range interaction between the tip and the sample. So, it is suggested that there is a strong electrostatic interaction between the tails and the AFM tip in neutral buffer of low salt concentration. When AFM tip approaches the CP surface of PM, it will induce a structural change of tails, as in the schematic shown in Figure 6b,c. As a result, the force dependent on the distance decays more slowly. After papain digestion, 5 negative surface charges per bR (Glu232, Glu234, Glu237, Asp242, and Ser248) are removed, with the loss of the 17 residues according to the folding model of bR since the cleavage occurs primarily between Gly-231 and Glu-232, and therefore the interaction between the AFM tip and the CP side is reduced and similar to that on the EC side. By far, further investigation is needed for a detailed model to test whether the hypothesis can explain our experimental result quantitatively.

Conclusions

Two types of different surface topography, flat and domelike, were observed when imaging PM with tapping-mode AFM under low salt concentration buffers. The domelike feature is not a real topography, but an artifact arising from variation in tip−sample interactions during AFM imaging. The papain-digestion experiment suggests that the domelike surface is the CP side of PM, while the flat surface is the EC side. Force curves show different electrostatic repulsive interactions between the tip and sample surfaces when measured on the two types of membrane surfaces. On the EC surface, the interaction follows the DLVO model, and relative surface charge density can be estimated by comparing measured membrane thickness under different buffer concentrations. On the CP surface, there is a strong tip−sample interaction with a much longer decay length than that predicted by the DLVO model. This interaction also leads to the formation of the domelike topography artifact due to a variation in the effective interaction area.

Supporting Information Available: Additional figure on PM topography and phase image. This material is available free of charge via the Internet at http://pubs.acs.org.

LA0631062